processes

MDPI

Article

The Casing Collapse Mechanism in Salt Formations in Deepwater Fields in Brazil

Chunwei Gu [1], Ming Xiang [1], Mengbo Li [2], Haifeng Zhu [1], Qinyue Zhang [1], Zixiao Xing [2], Mingchun Wang [2], Zhe Zhang [3,*] and Chuanliang Yan [3]

[1] CNOOC International Corporation, Beijing 100028, China; xiangming@cnoocinternational.com (M.X.)
[2] CNOOC Research Institute Co., Ltd., Beijing 100028, China
[3] School of Petroleum Engineering, China University of Petroleum (East China), Qingdao 266580, China
* Correspondence: b22020015@s.upc.edu.cn

Abstract: Salt formations are commonly encountered during oil and gas drilling. Due to the rheological properties of salt rocks, casing collapse accidents happen frequently. Under action of nonuniform geostress, casing failure has become an important influencing factor that restricts the exploration and development benefits of deep and ultra-deep wells. Casing stress in a period after well cementation in the salt formation of Brazilian deepwater fields was analyzed. Results show that the nonuniform geostress is instantaneously applied on the cement sheath when well cementation is completed in the salt formation and then transferred to the casing. Stress on the inner wall grows with an increase in the angle with the direction of the maximum horizontal principal stress and it reaches the maximum in the direction of the minimum horizontal principal stress. As the creep continues, stress on the inner wall of casings gradually enlarges and the circumferential stress in inner rings tends to be uniform, which means that creep of the formation weakens the nonuniformity of casing deformation. The collapse pressure on the outer wall of casings tends to increase at first and then decrease as the angle with the direction of maximum horizontal principal stress enlarges. Stress on the inner wall of casings in the salt formation reduces with the increasing thickness of casings selected, and the casing strength is improved as the wall thickness increases. The research results provide certain theoretical guidance for the strength check of casings in well cementation engineering in salt formations.

Keywords: geostress; salt rocks; creep; wellbore shrinkage

check for updates

Academic Editor: Qingbang Meng

Received: 14 December 2024
Revised: 16 January 2025
Accepted: 17 January 2025
Published: 22 January 2025

Citation: Gu, C.; Xiang, M.; Li, M.; Zhu, H.; Zhang, Q.; Xing, Z.; Wang, M.; Zhang, Z.; Yan, C. The Casing Collapse Mechanism in Salt Formations in Deepwater Fields in Brazil. *Processes* **2025**, *13*, 301. https://doi.org/10.3390/pr13020301

Copyright: © 2025 by the authors. Licensee MDPI, Basel, Switzerland. This article is an open access article distributed under the terms and conditions of the Creative Commons Attribution (CC BY) license (https://creativecommons.org/licenses/by/4.0/).

1. Introduction

Salt formations primarily consist of salt or gypsum. In the oil drilling industry, these formations are defined as those composed mainly of sodium chloride or other water-soluble inorganic salts, such as potassium chloride, magnesium chloride, and gypsum. Research indicates that salt rocks in sedimentary basins serve as ideal cap rocks, under which 80% to 90% of the world's oil and gas resources are located. In China, 40% of newly discovered oil and gas reserves are found beneath deep salt formations [1]. Consequently, salt formations are not only a major focus of the global oil industry but also critical regions for oil and gas resource development. However, the strong creep characteristics of salt rocks significantly hinder drilling and completion operations. During construction processes such as selecting drilling fluid density and designing casing strength, the creep behavior of salt rocks can lead to complex issues like wellbore instability, drilling tool jamming, and casing deformation. As a result, drilling in salt formations, particularly deep ones, poses a significant technical challenge [2].

Existing research on casing integrity in creeping formations mainly focuses on salt and soft mudstone formations [1,2]. Through theoretical calculations and numerical simulations, Yin et al. analyzed the casing load in creeping formations and concluded that the viscoelastic solution for casing load eventually converges to the elastic solution [2]. Thiemeyer N established a strength theory on the basis of Coulomb–Mohr strength theory and determined the properties of salt rocks, which are regarded as a kind of soft rock with a low strength and large deformation [1]. Liang constructed the strength curve equation in the form of Mohr–Coulomb criterion [3]. Yang et al. [4–6] were pioneers in investigating the impact of temperature (ranging from room temperature to 193 °C) on the creep rate of salt rocks. They performed triaxial creep tests on salt rocks under low confining pressure. The earliest high-pressure triaxial creep test on salt rocks was carried out in 1972, in which the maximum confining pressure reached 200 MPa. To meet the need for engineering research, lots of creep tests on salt rocks, including field and laboratory ones, have been conducted in the recent 20 years. Pollok conducted extensive uniaxial and triaxial tests on Asse salt rocks [7,8]. Freudenthal et al. [9–14], using various loading methods, such as single loading, staged loading, and constant-rate loading, carried out numerous laboratory and field tests to study the properties of salt rocks during the initial and steady-state creep stages. Tang et al. [15–18] examined the creep behavior of intercalated salt rocks by performing triaxial compressive creep tests on three types of core samples (salt rock intercalated with mudstone, pure mudstone, and pure salt rock) under varying confining pressures, aiming to understand their creep deformation patterns. Chen et al. [19] developed a two-dimensional (2D) finite element or finite difference model to evaluate casing loads in salt formations subjected to horizontal geostress. Deng et al. [20–23] analyzed the effects of mineral composition, deviatoric stress, temperature, and confining pressure on creep behavior and proposed a constitutive equation for the steady-state creep rate based on creep curves and rock parameters. WG Liang et al. [24] established a three-dimensional (3D) finite element and finite difference model to study the mechanical behavior of casings in salt formations under 3D geostress conditions. Bu et al. [25–27] introduced a step-by-step simulation approach to analyze the mechanical state of wellbores during drilling and cementation processes. Ma et al. [28–31] created a finite element model for deviated wellbores in salt formations, investigating the effects of wellbore inclination and azimuth on shrinkage and casing stress. Recent research focused on casing deformation and stress in vertical wellbores under nonuniform geostress, incorporating the deepwater pre-salt geostress conditions of Brazil's Santos Basin. This study integrates laboratory creep experiments with theoretical analysis to establish a creep constitutive model suitable for Brazil's Santos Basin. The developed creep criterion is coupled with the UMAT subroutine and incorporated into the finite element analysis software ABAQUS 2022, thereby achieving a seamless integration of experimental and theoretical approaches (ABAQUS: Version 2022, Dassault Systèmes, Vélizy-Villacoublay, France).

The research methodology of this study is shown in Figure 1. In this paper, the casing collapse mechanism and casing design of salt rock formation in Santos Basin of Brazil will be studied according to the steps of the research methodology.

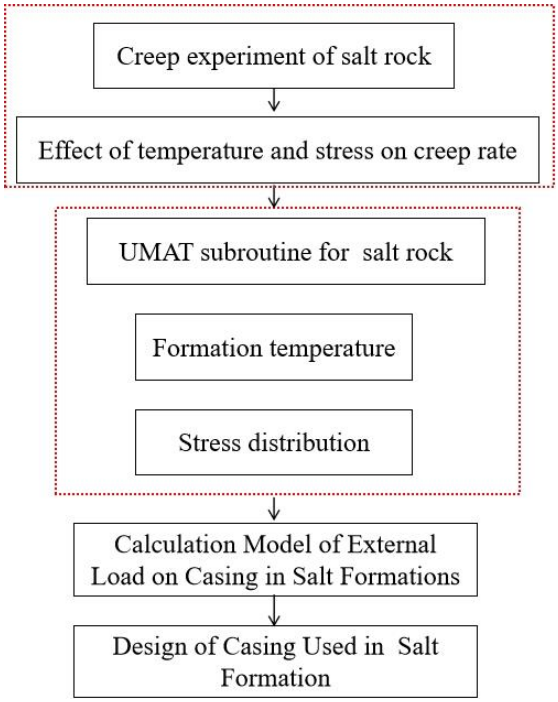


Figure 1. Research methodology.

2. Mathematical Models

2.1. Creep Laws

Creep is the process by which material deformation evolves over time when subjected to a constant applied load. In creep tests conducted on materials in the elastic state, the total strain can be expressed as the sum of elastic strain and creep strain [32], represented as:

$$\varepsilon(t) \quad = \varepsilon_e + \varepsilon_c \tag{1}$$

In Equation (6), ε(t) represents the total strain, ε_e denotes the elastic strain, and ε_c is the creep strain, which is influenced by temperature (T), time (t), and stress σ [33]. The relationship can be written as:

$$\varepsilon_e \quad = f(\sigma, t, T) \quad = f_1(\sigma)\, f_2(t)\, f_3(T) \tag{2}$$

Researchers, both in China and abroad, have developed a series of constitutive models to describe the long-term mechanical behavior of salt rocks. Due to the relatively small size of a wellbore compared to the vast spatial scale of thick salt formations, wellbore shrinkage can be viewed as a form of creep occurring under fixed temperature and load conditions. Hunsche U [33] highlighted that, at high temperatures, the creep activation energy matches the atomic self-diffusion activation energy, indicating that vacancy diffusion is the primary mechanism governing the strain rate. Building on this insight, Weertman formulated the constitutive equation for steady-state creep rate:

$$\varepsilon_e = \frac{A}{m+1}\sigma^n f_3(T) \tag{3}$$

$f_1(\sigma)$ $f_2(t)$ is simplified as the Norton power method related to time, of which the initial and second creep stages can be expressed as [34]:

$$\varepsilon_e = f(\sigma, t) = \frac{A}{m+1}\sigma^n t^{m+1} f_3(T) \tag{4}$$

By differentiating Equation (4) with respect to time, the Norton power law, which is related to creep time, can be derived.

$$\frac{d\varepsilon_c}{dt} = A\sigma^n t^m f_3(T) \tag{5}$$

According to Gunther R. M. et al. [34], salt rock cores collected from Brazilian Santos Basin at a depth of 4102.99 m were used to conduct creep tests at 25 °C, 50 °C, and 75 °C for 21 d. Based on the obtained test curves in Figures 2–4, the creep constitutive equation of salt rocks is [15]:

$$\frac{d\varepsilon_c}{dt} = 4.48 \times 10^{-10} \cdot t^{0.5167} \cdot \sigma^{3.8} \cdot T^{2.2890} \tag{6}$$

Test data of Gunther R. M. et al. [34] were all obtained from rock cores taken from the extremely thick strata in Brazilian Santos Basin and, therefore, are accurate and reliable. The strain at the boundary between the decelerated and steady-state creep stages also decreases. Fortran language is used to compile the UMAT subprogram to embed the above creep constitutive model of salt rocks into the finite element analysis tool ABAQUS 2022. Figure 2 shows a triaxial testing machine on which we can carry out long-term creep experiments. As shown in Figure 3, with the increase in applied load, the creep rate of salt rock decreases in the deceleration creep stage but increases in the steady creep stage. The creep rate of salt rock also increases with the increase in temperature. We fit the curves in Figures 3–5 to obtain the parameters in the creep criteria.

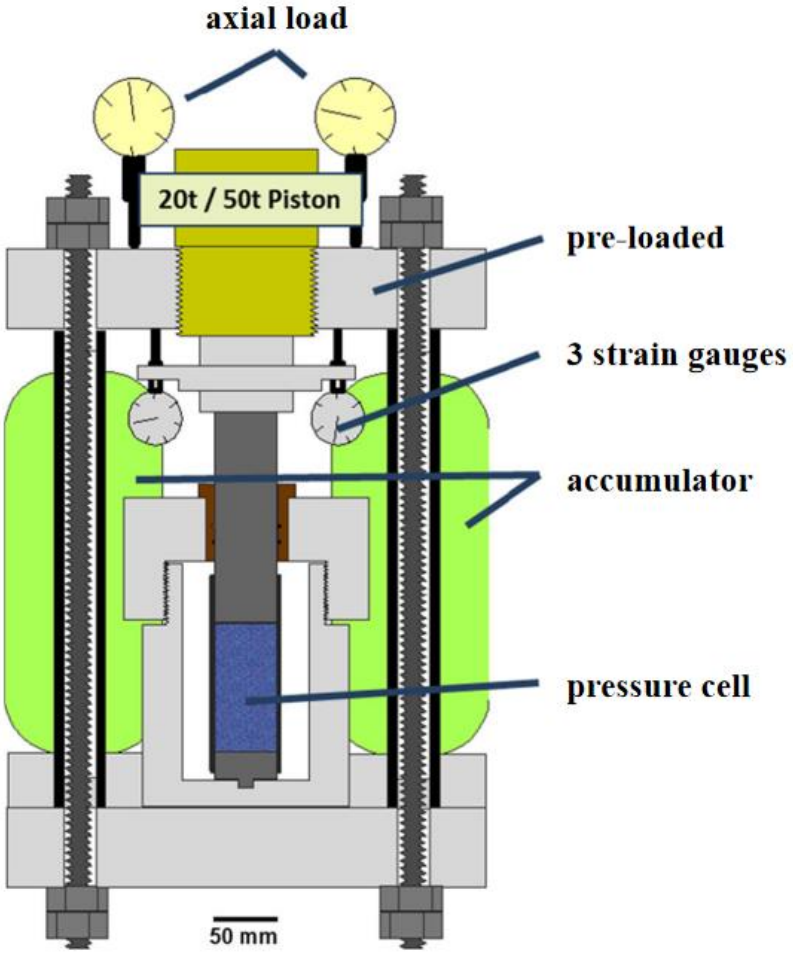


Figure 2. The triaxial device for long-term creep terms.

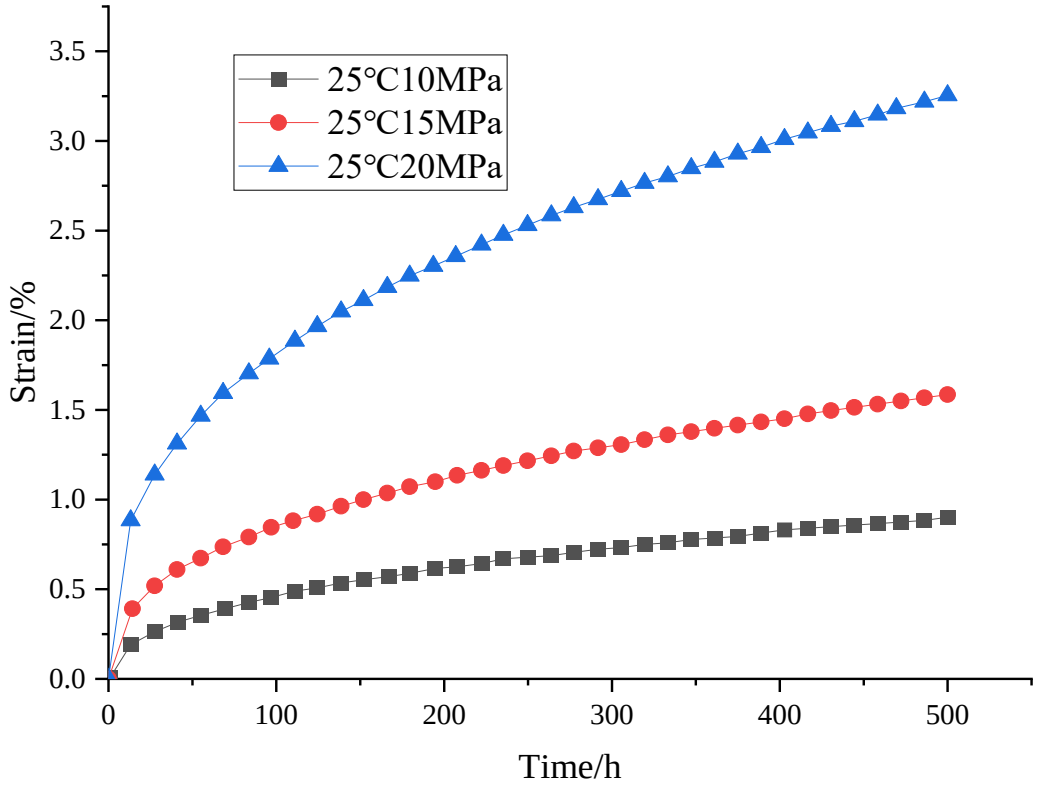


Figure 3. Fitting results of the creep model of salt rocks at 25 °C.

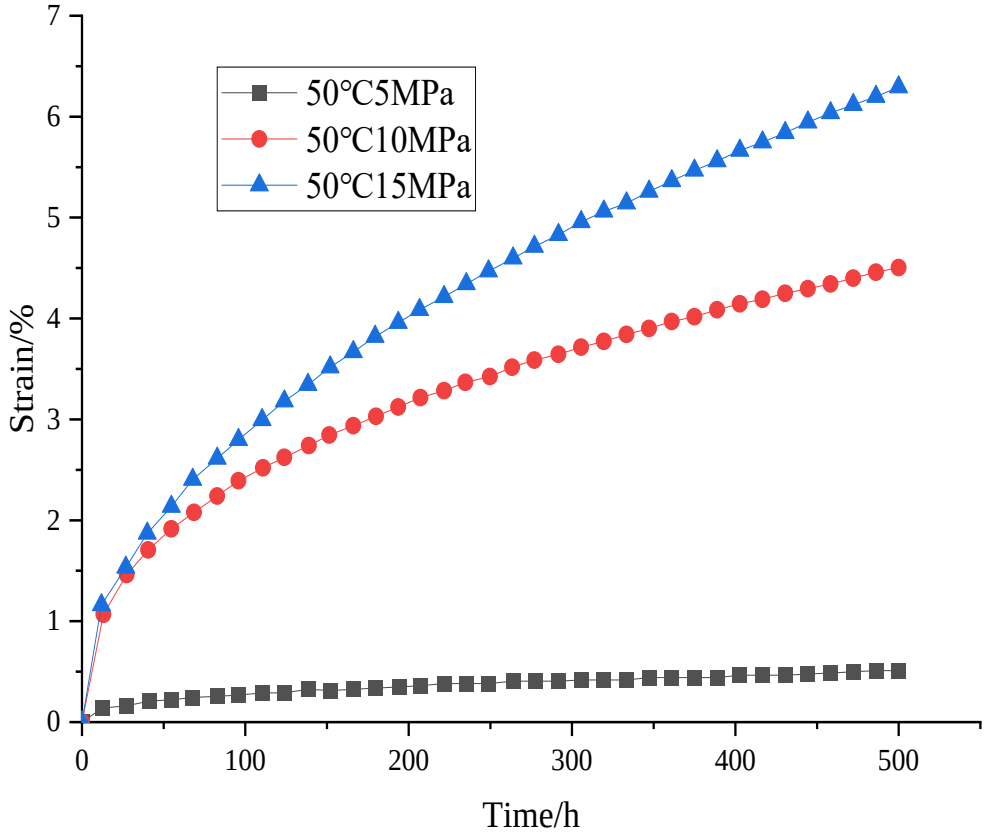


Figure 4. Fitting results of the creep model of salt rocks at 50 °C.

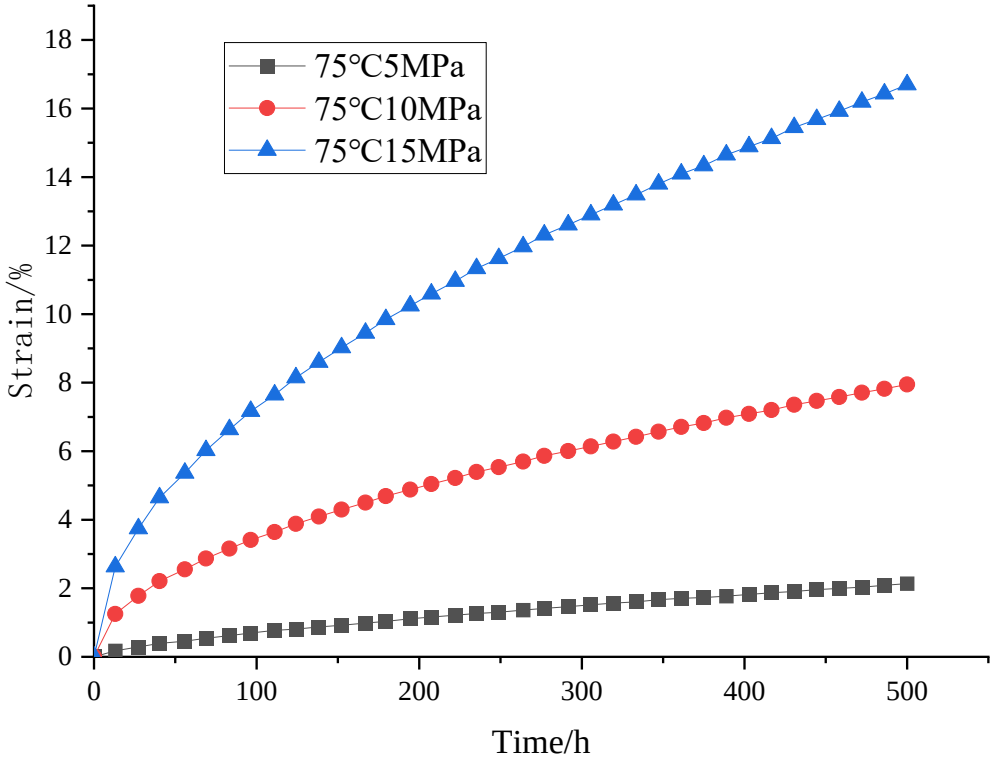


Figure 5. Fitting results of the creep model of salt rocks at 75 °C.

2.2. Calculation Model of External Load on Casing in Salt Formations

Due to the rheological properties of formations, the stress around wellbores constantly changes after well cementation, so the collapse pressure applied by salt rocks on the casing also changes all the time. For the convenience of study on changes in the collapse pressure applied by strata with a mudstone interlayer on the casing, the following assumptions are made for relationships among the formation, casing, and cement sheath [35]:

(1) During the creep process, the volume of the rocks remains constant and the hydrostatic pressure does not influence the creep behavior of salt rocks.
(2) The wellbore is well cemented with the casing and no micro-fractures are developed in the creep process of formations.
(3) The strain rate and stress tensor share the same principal direction.
(4) In the creep process of formations, the cement sheath is simplified as an elastomer and its plastic deformation is not considered. The cement sheath only plays a role in transferring the load, while influences of its size and elastic parameters on the stiffness of casing under external load are negligible; after casing cementation in deep formations, the axial deformation is inhibited.

Assuming that geostress is uniformly distributed along the axial direction of casings, then the problem is simplified as a problem to calculate the external load on flat casings. As shown in Figure 6, the outer boundary of the model is circular, on which uniform principal stress is applied. Under action of the far-field stress field P_o and liquid-column pressure in casings P_i, the collapse pressure on casings gradually ramps up due to creep of formations, which is the function of time t, that is, $P_a(t)$. The model is composed of three parts, namely, the casing, cement sheath, and salt formation.

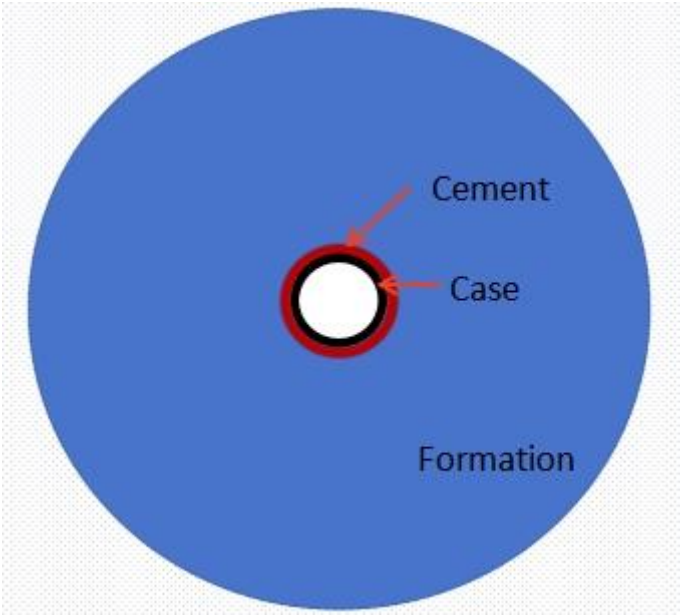


Figure 6. Mechanical model of the casing–cement sheath-formation combination.

According to the above assumptions, casing stress can be obtained after applying load on the combination using the formula for radial displacement of thick-walled cylinders and the elastic theory:

$$\begin{aligned} \sigma_r(r,t) &= \frac{b^2 p_i}{a^2-b^2}\left(1-\frac{a^2}{r^2}\right) - \frac{b^2 p_a(t)}{a^2-b^2}\left(1-\frac{b^2}{r^2}\right) \\ \sigma_\theta(r,t) &= \frac{b^2 p_i}{a^2-b^2}\left(1+\frac{a^2}{r^2}\right) - \frac{b^2 p_a(t)}{a^2-b^2}\left(1+\frac{b^2}{r^2}\right) \end{aligned} \tag{7}$$

In Equation (7), a is the inner diameter of wellbores; b is the inner diameter of casings; and r is the distance from the research point to the wellbore axis [35]. Under the action of liquid-column pressure in casings P_i and collapse pressure $P_a(t)$, the radial displacement of the outer wall of casings in the combination is:

$$\begin{aligned} U_1(a,\ t) &= k_{ic} p_i - k_{rc} p_a(t) \\ k_{ic} &= \frac{a(1+\mu_c)(2-2\mu_c)b^2}{E_c(a^2-b^2)} \\ k_{rc} &= \frac{a(1+\mu_c)\left((1-2\mu_c)a^2+b^2\right)}{E_c(a^2-b^2)} \end{aligned} \tag{8}$$

In Equation (8), E_c is the elastic modulus of casings; μ_c is the Poisson's ratio of casings; K_{ic} is the burst stiffness of casings; and K_{rc} is the collapse stiffness of casings. The counter-force of casings against strata $P_a(t)$ and the formation external pressure P_o cause the wellbore wall to have radial rebound displacement [35,36]:

$$\begin{aligned} U_2(a,\ t) &= k_{is} p_a(t) - k_{rs} p_0 \\ k_{is} &= \frac{a(1+\mu_s)}{E_s} \\ k_{rs} &= \frac{a(1+\mu_s)(2-2\mu_s)}{E_s} \end{aligned} \tag{9}$$

where E_s is the elastic modulus of salt formations; μ_s is the Poisson's ratio of salt formations; K_{is} is the burst stiffness of salt formations; and K_{rs} is the collapse stiffness of salt formations. The formation can be regarded as a thick-walled cylinder of infinite thickness. Under the external pressure P_o and internal pressure $P_a(t)$, its inner wall has creep displacement U(t) inward of the wellbore. The application of uniform geostress can be simplified as a plane

strain problem, which is also an axisymmetric stress problem. Under the polar co-ordinates, the creep rate component is expressed as follows [36]:

$$\begin{gathered}\mathcal{E}'_\theta = \frac{\sqrt{3}}{2} A exp\left(-\frac{Q}{RT}\right) sinh\left(\frac{\sqrt{3}}{2} B(\sigma_\theta - \sigma_r)\right) \\ \varepsilon'_r = -\varepsilon_\theta\end{gathered} \tag{10}$$

The boundary conditions are [36,37]:

$$\begin{gathered}\sigma_{r=a} = p_i \\ \sigma_{r\to\infty} = \sigma_H\end{gathered} \tag{11}$$

Considering the continuity and compatibility of the casing–formation interface, there is the following relationship [37]:

$$|U_c(t)| - |U_2(a,t)| = |U_1(a,t)| \tag{12}$$

By substituting the expression of displacement, the following relationship between external load on casings and geostress can be attained [37]:

$$k_{ic} p_i - k_{rc} p_a(t) = U_c(t) - (k_{is} p_a(t) - k_{rs} p_0) \tag{13}$$

The stress difference on the inner wall of the thick-walled cylinder of infinite thickness is [37]:

$$\sigma_\theta - \sigma_r = 2(p_0 - p_a(t)) \tag{14}$$

The above calculation of casing stress is only applicable to non-ruptured rheological formations with a small dip angle. Structured grids are both used for the cement sheath and salt formation, which are refined in the vicinity of the wellbore. The grid size of elements of salt rocks near the wellbore is set to be 0.01 m. Based on the commercial finite element software ABAQUS 2022, the constitutive models, boundary conditions, and edge loads are embedded in ABAQUS using the secondary development function DLOAD and DISP subprogram. Then, the change process of displacement in the creep process of underground salt rocks and its influence on wellbore deformation are computed.

3. Analysis of External Load on Casings in Extremely Thick Salt Formations in Brazilian Deepwater

3.1. Stress Analysis of Casings in Salt Formations in Brazilian Deepwater Fields

Wellbore P is located in Santos Basin in Brazil where the water depth is 2285 m and its design depth is 5366 m. Geological prediction shows that the salt formation is 2606 m thick. Data of formation temperature in the block of wellbore P are shown in the Figure 7.

The geostress profile was computed using the seismic interval velocity and the horizontal structural stress coefficient obtained by inversion. Based on the actual geological parameters, various parameters in the finite element model are set in Table 1 [37].

Geostress equilibrium is crucial for accurately simulating the drilling process. To ensure that the initial stress loading aligns with the geostress equilibrium principle, the salt formation must only withstand the initial stress without undergoing significant initial deformation.

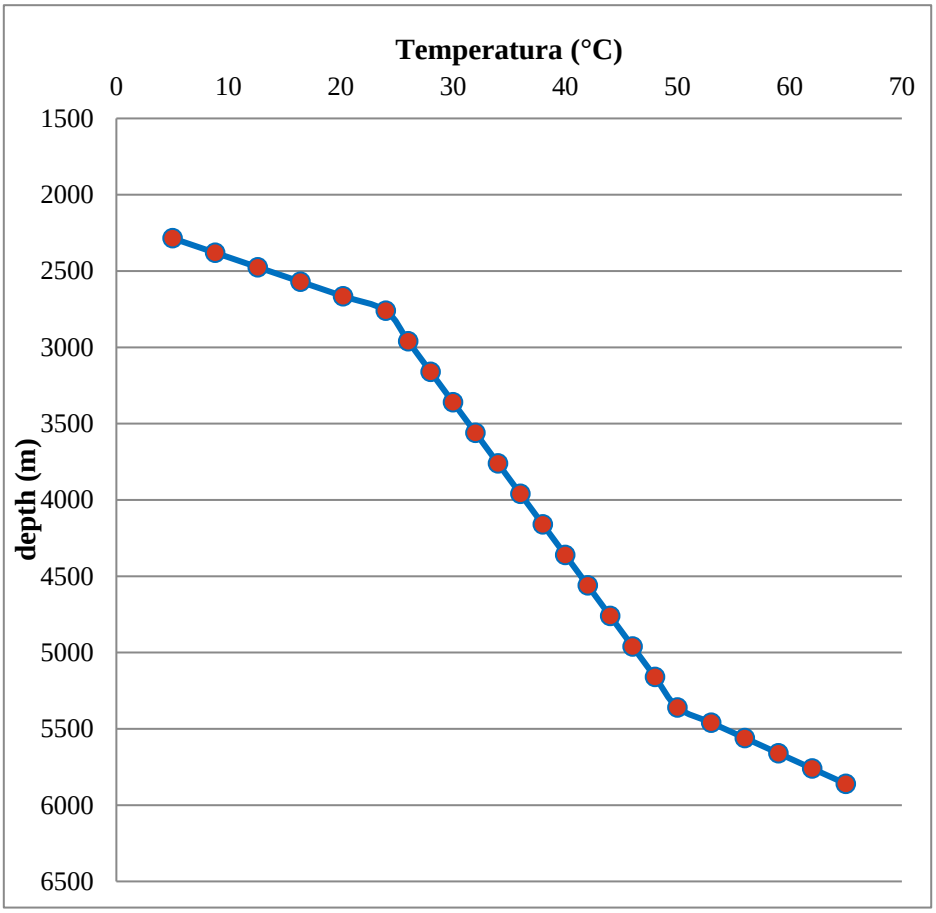


Figure 7. Formation temperature in the block of wellbore P.

Table 1. Basic parameters of formations.

Model Parameters	Values
Seawater density/(g/cm^3)	1.03
Mudstone density/(g/cm^3)	2.2
Density of salt rocks/(g/cm^3)	2.1
Young's modulus (GPa)	10
Depth of the top of salt formations/m	2760
Depth of the bottom of salt formations/m	5366
Temperature of the bottom of salt formations/°C	49
Poisson's ratio	0.3
Wall thickness of casings/mm	8.38
Burial depth/m	3000

The analysis step of geostress equilibrium is set to be geostatic. The geostress analysis step is generally an implicit analysis process of static force, which simulates the stress distribution in formations not disturbed by the drill bit. Therefore, conditions of the wellbore and far-field boundary displacement need to be set in the analysis step. Figure 8 shows the results after reaching geostress equilibrium, in which the maximum displacement in the model is only 2.12×10^{-15} mm, geostress reaches equilibrium, and boundary conditions are smoothly imposed to the model. This indicates that the initial boundary conditions are effective and feasible in the subsequent analysis.

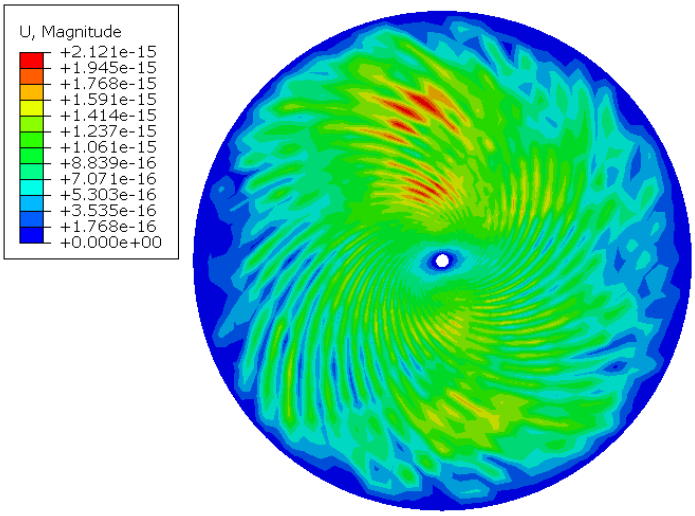
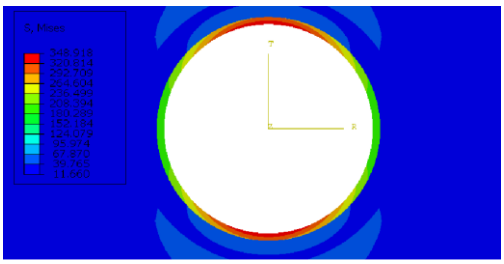
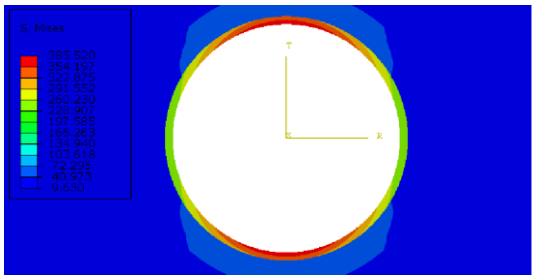


Figure 8. Geostress equilibrium.

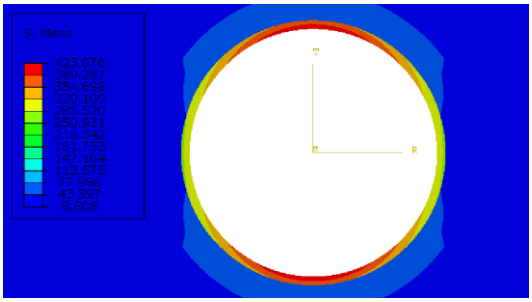
The displacement constraint on the wellbore needs to be relieved in the second step, namely, VSICO analysis. Under nonuniform geostress, the formation, casing, and cement sheath come into close contact, the casing and cement sheath are well cemented, and the external load on the casing is mainly caused by creep of the salt formation under geostress. The external load generated by creep of the formation is transferred from the salt formation to the cement sheath, from which it is then applied to the outer wall of the casing. As a result, a contact pressure is generated on the outer wall of the casing and the inner wall of the cement sheath, and the maximum stress on the casing is found on the inner wall. X and Y are set as the directions of the maximum and minimum horizontal principal stresses, respectively. To further show changes in the radial displacement during creep of salt rocks, the Mises stress nephograms, radial stress nephograms, and deformation nephograms of the casing in the salt formation at different moments were drawn. Figure 9 shows the Mises stress nephograms, Figure 10 shows the circumferential path on the casing wall, and Figure 11 shows the Mises stress distribution on the inner wall of casings.



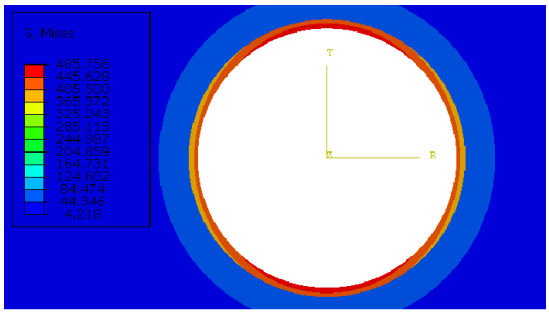
(**a**) Well cementation



(**b**) One month after well cementation



(**c**) One year after well cementation



(**d**) Ten years after well cementation

Figure 9. Mises stress nephograms.

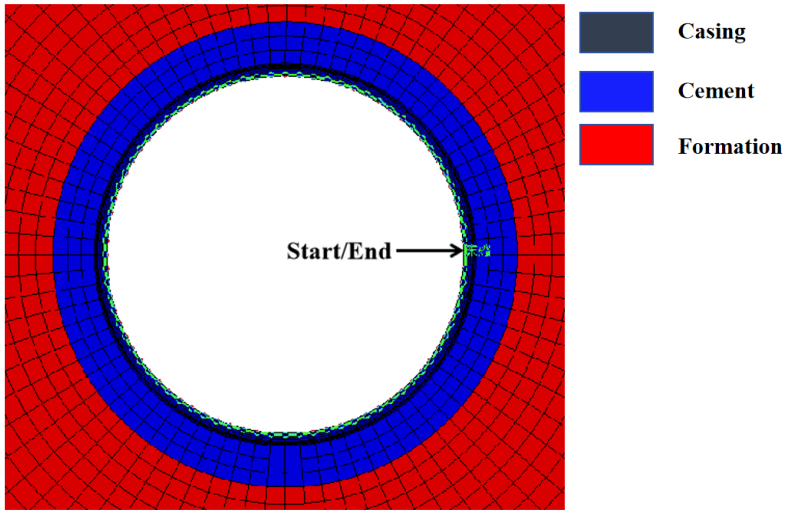


Figure 10. Circumferential path on the casing wall.

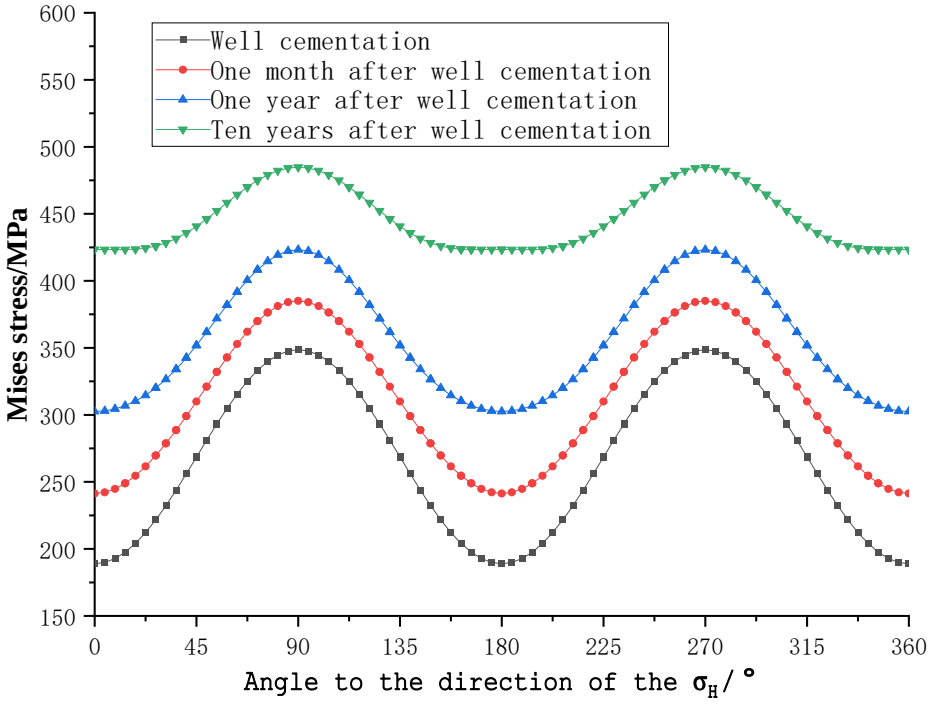
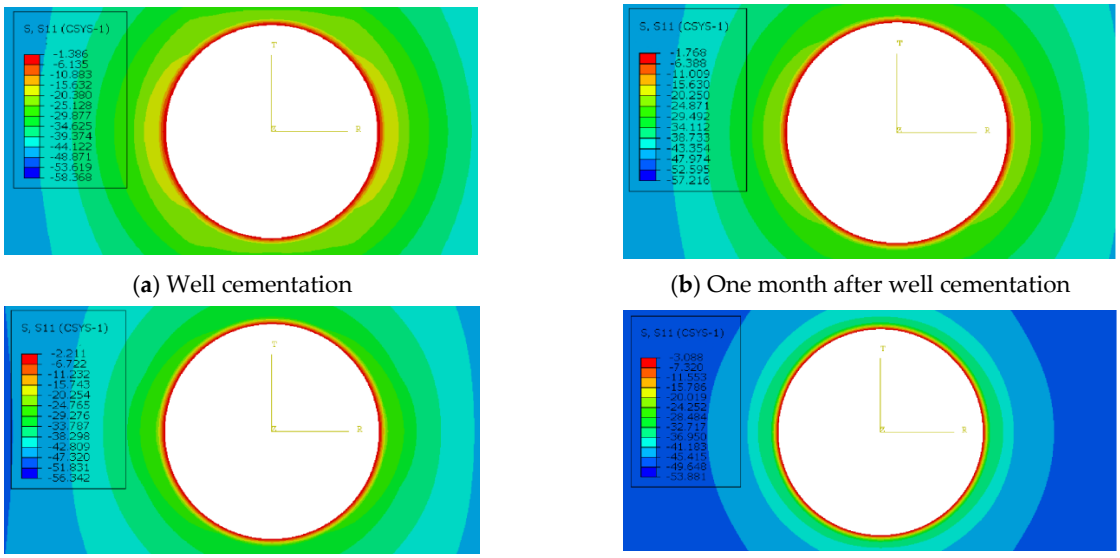


Figure 11. Mises stress distribution on the inner wall of casings.

Casing deformation is a progressive process. To quantitatively study the stress and deformation characteristics of the casing under nonuniform geostress, nodes on a circumferential path of the casing are selected to extract and analyze physical quantities at these nodes. The starting point of the path corresponds to the direction of the maximum horizontal principal stress and the end of the path coincides with the starting point. The circumferential path separately experiences the maximum and minimum horizontal principal stresses. Figure 12 shows the radial stress nephograms.

Change curves of Mises stress on the outer wall of casings with time are illustrated in Figure 13. When well cementation is completed, the nonuniform geostress is instantaneously applied to the cement sheath and then transferred to the casing. The Mises stress on the inner wall grows with an increase in the angle with the direction of the maximum horizontal principal stress. When the angle is 0°, the Mises stress on the inner wall of casings is 349 MPa; when the angle is 90°, the Mises stress on the inner wall is 486 MPa. Obviously, the casing is most likely to be damaged along the direction of the minimum

principal stress in the elastic deformation stage. As the creep continues, the Mises stress on the inner wall of casings gradually ramps up, while its value tends to be uniform. When the stress is relatively uniformly distributed on casings, it needs to check the collapsing strength of the casing. Figure 14 shows the collapse pressure on the outer wall of casings 30 days after well cementation. It can be seen from Figures 14 and 15 that, in the elastic deformation stage of the formation, the collapse pressure on the casing reaches the maximum in the direction of the minimum horizontal principal stress and the minimum in the direction of the maximum horizontal principal stress. As the creep further proceeds, the distribution of collapse pressure on the outer wall of casings changes, and its value tends to increase at first and then decrease with the enlargement in the angle with the direction of the maximum horizontal principal stress.



(**a**) Well cementation (**b**) One month after well cementation

(**c**) One month after well cementation (**d**) Ten years after well cementation

Figure 12. Radial stress nephograms.

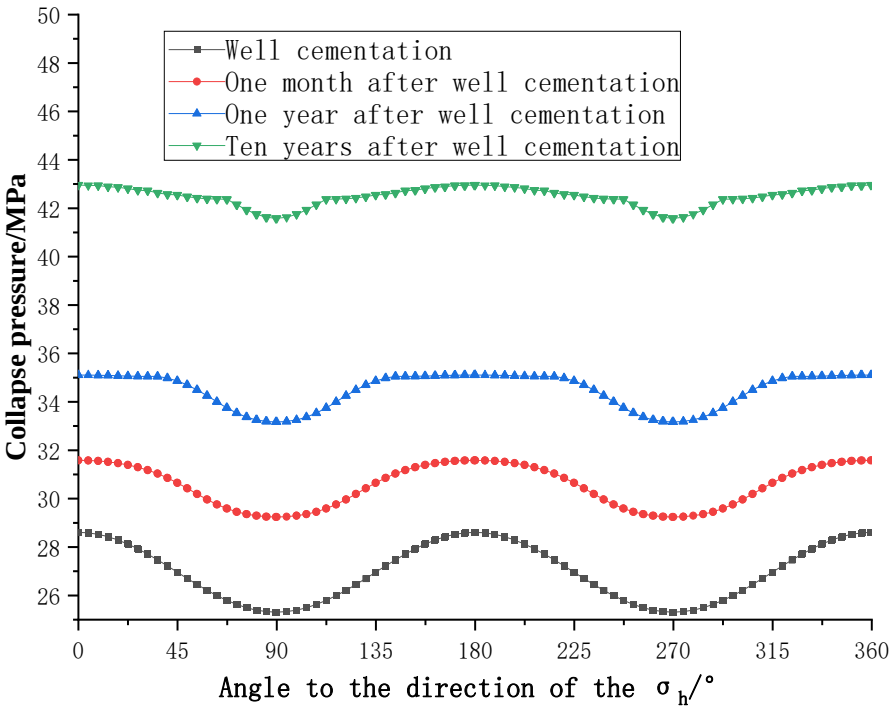
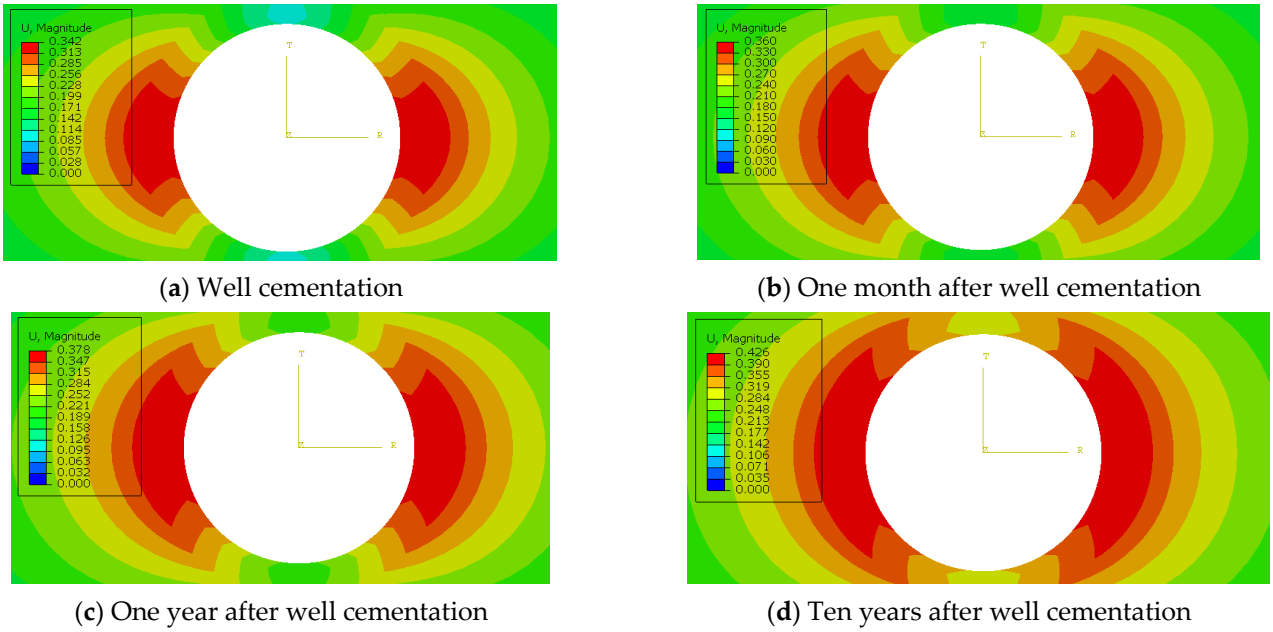


Figure 13. Collapse pressure on the casing at different moments.



(**a**) Well cementation (**b**) One month after well cementation

(**c**) One year after well cementation (**d**) Ten years after well cementation

Figure 14. Displacement nephograms.

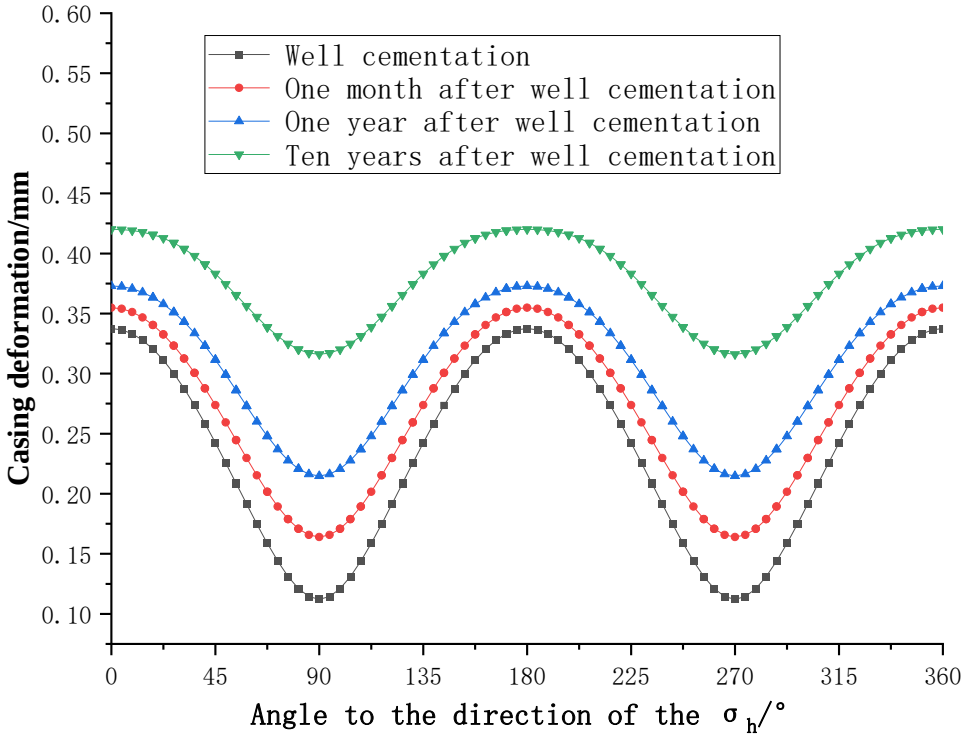


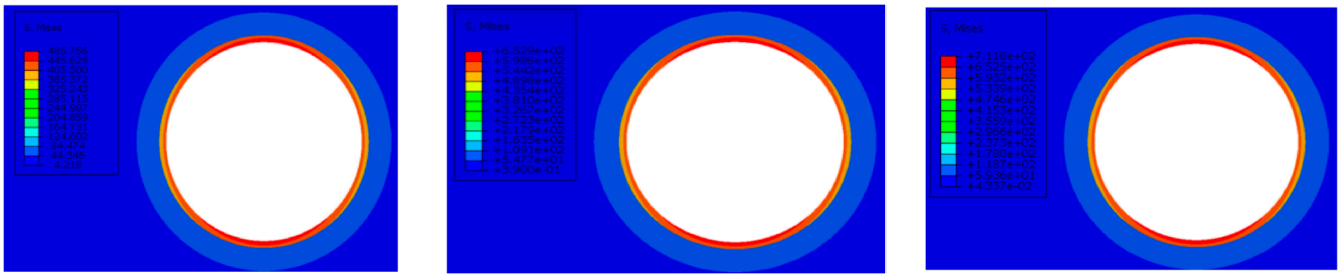
Figure 15. Casing deformation at different moments.

3.2. Sensitivity Analysis of Casing Strength

3.2.1. Influence of Burial Depth on Casing Stress

Casing deformation is a process accruing over time. For creeping formations, when rocks creep, the casing begins to bear the collapse pressure and shrinks inward. In salt formations, the geostress is mainly derived from the pressure of overlying formations and the tectonic force generated in tectonic movements. After finishing well cementation, such tectonic force becomes the power that drives creep of rocks to extrude the casing. Moreover, with the increasing depth of formations, the formation temperature also rises and the creep rate of rocks also accelerates. Therefore, as the depth increases, the casing stress enlarges

accordingly. The Mises stress nephograms of the casing at different depths is shown in Figures 16 and 17, showing the change curves of casing Mises stress with the depth.



(**a**) 3000 m (**b**) 4030 m (**c**) 5060 m

Figure 16. Mises stress nephograms of the casing at different depths.

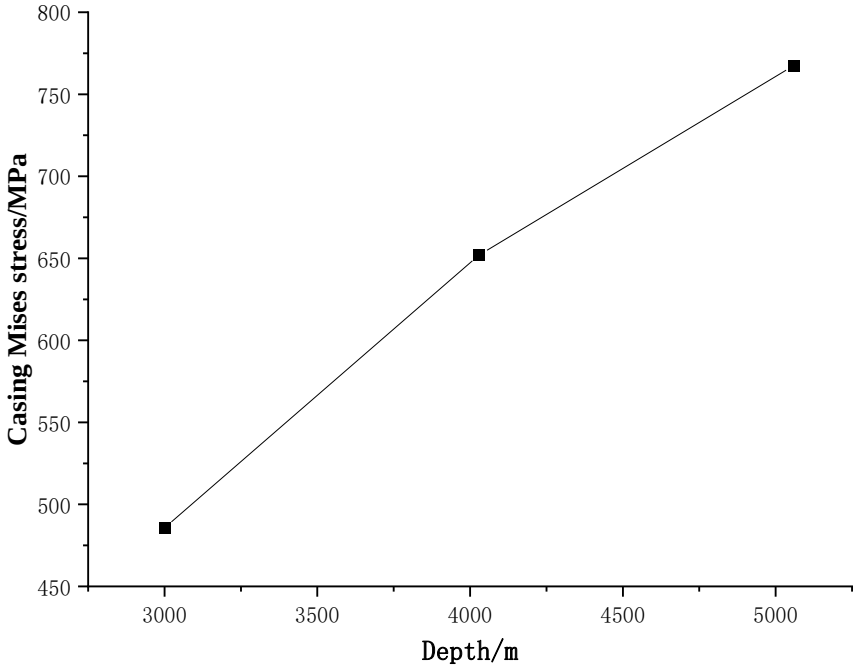
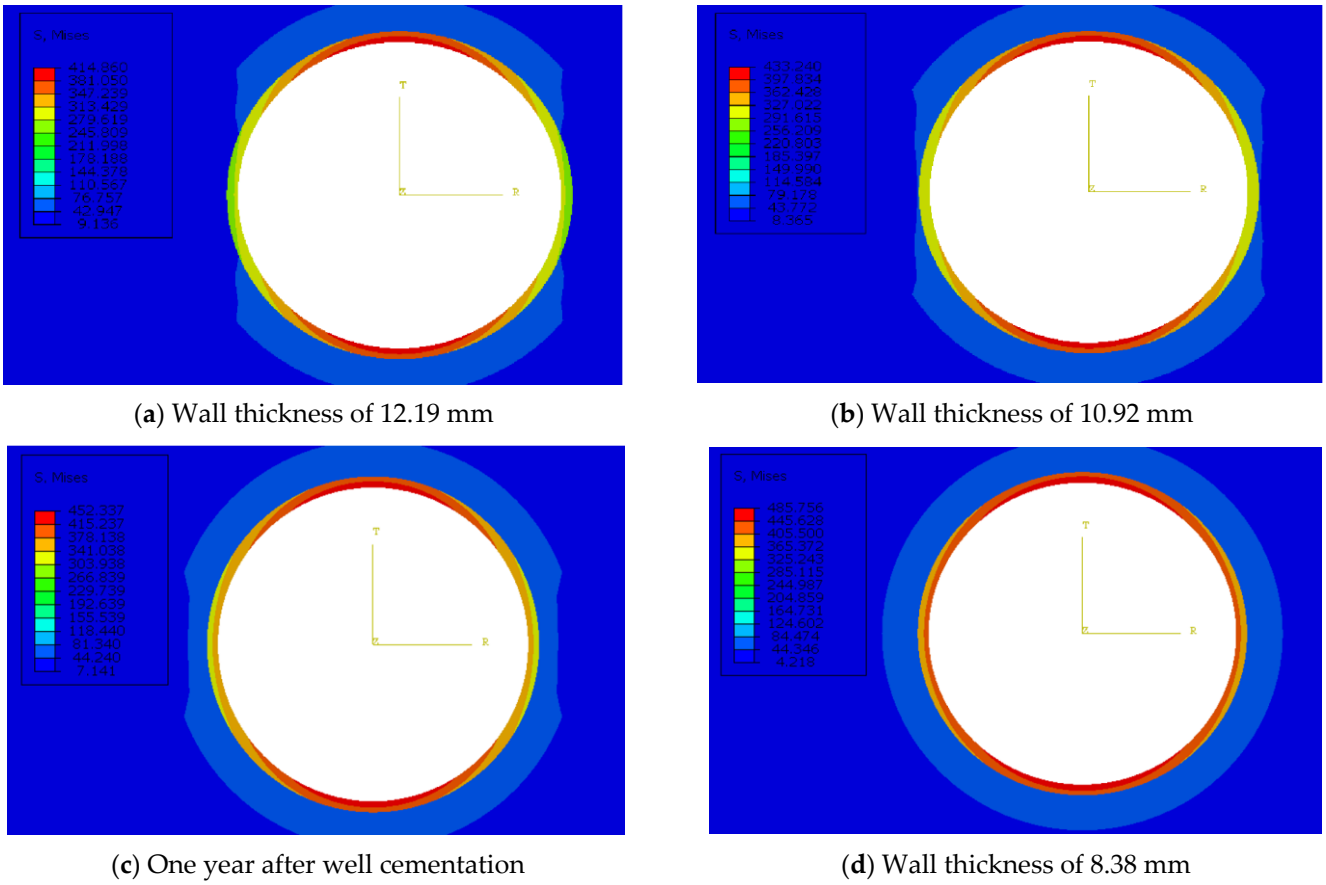


Figure 17. Change curves of casing Mises stress with the depth.

3.2.2. Influence of Wall Thickness of the Casing on Casing Stress

When applying collapse pressure onto the casing wall to reach the yield strength of the casing, the casing body undergoes plastic deformation. Under the condition, it is regarded unsafe. In accordance with the API standard, four wall thickness standards are available for the corresponding casing of wellbores, namely, 8.38, 9.65, 10.92, and 12.19 mm. Figure 16 displays the Mises stress on the inner wall of casings with different wall thicknesses 10 years after well cementation, which shows that the Mises stress on the inner wall decreases with the increasing thickness of the casing selected. Therefore, it is concluded that increasing the wall thickness of casings is an effective approach to improve the collapse resistance. The Mises stress nephograms of casings with different wall thicknesses is shown in Figure 18. The Figure 19 shows the wall thickness–stress curves in different directions.



(**a**) Wall thickness of 12.19 mm (**b**) Wall thickness of 10.92 mm

(**c**) One year after well cementation (**d**) Wall thickness of 8.38 mm

Figure 18. Mises stress nephograms of casings with different wall thicknesses.

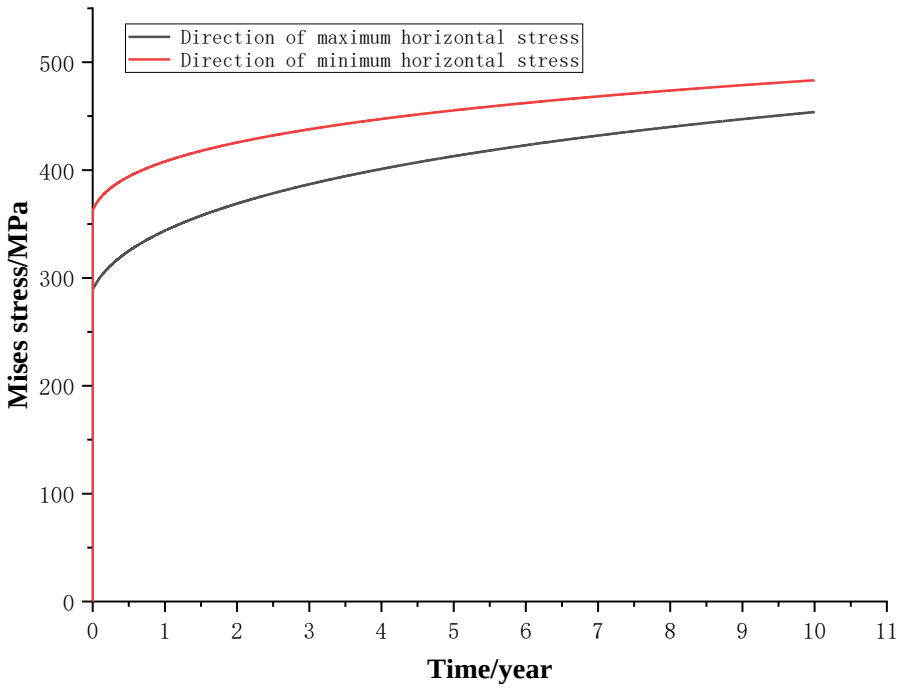


Figure 19. Wall thickness–stress curves in different directions.

The nonuniform load caused by creep of salt formations is one of the main causes for casing failure. The magnitude of nonuniform geostress is related to the burial depth of casings. When the geostress gradient remains unchanged while increasing the formation depth from 3000 m to 4030 m and 5060 m, influences of the geostress on casing stress and

service life in the salt formation are explored. The most straightforward method to prevent casing deformation is to improve the steel grade and increase the thickness of casing, which, however, will substantially increase well construction costs. Therefore, it needs to check the casing strength at different depths of salt formations to select the optimal wall thickness and steel grade of casings while ensuring the well cementation quality. Figure 20 shows the change curves of casing stress with wall thickness at different burial depths of salt formations.

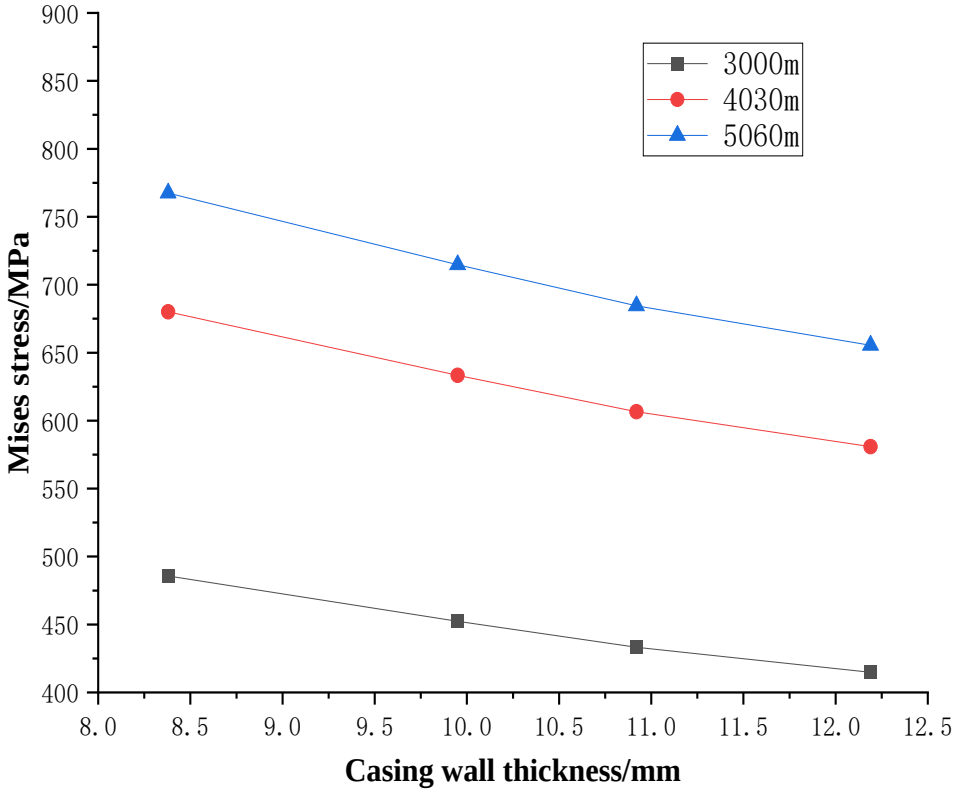


Figure 20. Change curves of casing stress with wall thickness at different burial depths of salt formations.

4. Design of Casing Used in the Extremely Thick Salt Formation in Brazilian Deepwater

As the amount of development of pre-salt reservoirs is increasing day by day and the geological conditions become increasingly harsh, higher requirements are set for the resistance of casings to external load. In the meantime, the demand for high-steel-grade casings also increases. The steel grade of oil-well casings stipulated in API Spec 5CT—2011 (Casing and Tubing) is divided into four groups according to the working condition [38–40], in which Q125 and Q-125HC oil-well casings belong to high-strength high-toughness casings. They are manufactured through a seamless or welding process and subjected to full-length quenching plus tempering treatment selected by the manufacturer. When using such oil-well casings, the well cementation cost is extremely high. Therefore, to meet the market demand, adapt to the working condition of oilfields, and save development cost, casings in the upper, middle, and lower horizons of salt formations need to be designed to ensure that the casing strength in the salt formation meets the compression requirement of extremely thick salt formation (Tables 2–4).

Table 2. Casing stress in the upper horizon (3000 m) of wellbore P in the salt formation 10 years after well cementation and casing selection.

Wall Thickness of Casings/mm	Stress/MPa	Optional Steel Grade of Casings (Safety Factor: 1.125)
8.38	485.76	N-80, C90, C-95, VM95HC, Q-125, Q-125HC
9.95	452.34	N-80, C90, C-95, VM95HC, Q-125, Q-125HC
10.92	433.24	N-80, C90, C-95, VM95HC, Q-125, Q-125HC
12.19	414.86	N-80, C90, C-95, VM95HC, Q-125, Q-125HC

Table 3. Casing stress in the middle horizon (4030 m) of wellbore P in the salt formation 10 years after well cementation and casing selection.

Wall Thickness of Casings/mm	Stress/MPa	Optional Steel Grade of Casings (Safety Factor: 1.125)
8.38	680.06	P-110, Q-125, Q-125HC
9.95	633.27	P-110, Q-125, Q-125HC
10.92	606.54	P-110, Q-125, Q-125HC
12.19	580.81	C-95, VM95HC, P-110, Q-125, Q-125HC

Table 4. Casing stress in the lower horizon (5060 m) of wellbore P in the salt formation 10 years after well cementation and casing selection.

Wall Thickness of Casings/mm	Stress/MPa	Optional Steel Grade of Casings (Safety Factor: 1.125)
8.38	767.49448	Q-125, Q-125HC
9.95	714.69246	P-110, Q-125, Q-125HC
10.92	684.5192	P-110, Q-125, Q-125HC
12.19	655.4788	C-95, VM95HC, P-110, Q-125, Q-125HC

5. Conclusions

(1) When well cementation in salt formations is completed, the nonuniform geostress is instantaneously applied to the cement sheath and then transferred to the casing. The Mises stress on the inner wall of casings in salt formations grows with the enlargement of the angle with the direction of the maximum horizontal principal stress and reaches the maximum in the direction of the minimum horizontal principal stress. The stress on casings in the direction of the minimum horizontal principal stress is lower than that in the direction of the maximum horizontal principal stress.

(2) As the creep continues, the Mises stress on the inner wall of casings gradually ramps up while its value tends to be uniform, which means that the creep of formations weakens the nonuniformity of casing deformation. The Mises stress on the casing wall grows with the increasing burial depth of casings.

(3) In the elastic deformation stage of salt formations, the collapse pressure on casings reaches the maximum in the direction of the minimum horizontal principal stress and the minimum in the direction of the maximum horizontal principal stress. Whereas, as the creep continues, the distribution of collapse pressure on the outer wall of casings changes and its value tends to increase at first and then decrease with the enlargement in the angle with the direction of the maximum horizontal principal stress.

(4) The Mises stress on the inner wall of casings in salt formations declines and the casing strength is improved with the increasing thickness of casings selected. To meet the requirement for the collapsing strength of casings, it needs to enlarge the wall thickness and increase the steel grade of casings. This research checked the strength of casings used for well cementation in the salt formation section of wellbore P in Brazilian Santos Basin and selected the optimal steel grade and wall thickness for the casings in the salt formation.

Author Contributions: Methodology, C.Y.; Software, M.L., H.Z., Z.X., M.W. and Z.Z.; Validation, M.X.; Formal analysis, Q.Z.; Supervision, C.G. All authors have read and agreed to the published version of the manuscript.

Funding: This research received no external funding.

Data Availability Statement: The original contributions presented in this study are included in the article. Further inquiries can be directed to the corresponding author(s).

Conflicts of Interest: Authors Chunwei Gu, Ming Xiang, Haifeng Zhu and Qinyue Zhang were employed by the company CNOOC International Corporation. Authors Mengbo Li, Zixiao Xing and Mingchun Wang were employed by the company CNOOC Research Institute Co., Ltd. The remaining authors declare that the research was conducted in the absence of any commercial or financial relationships that could be construed as a potential conflict of interest.

References

1. Thiemeyer, N. Microfabrics and Deformation Mechanisms of Gorleben Rock Salt. Ph.D. Thesis, Universitätsbibliothek Johann Christian Senckenberg, Frankfurt, Germany, 2015.
2. Yin, Y.; Chen, Z.; Li, P. Theoretical solutions of stress distribution in casing-cement and stratum system. *Chin. J. Theor. Appl. Mech.* **2006**, *38*, 835–842.
3. Liang, W.; Xu, S.; Mo, J.; Wu, D.; Zhang, C. Experimental Study on the Strain Rate Effect of the Mechanical Properties of Rock Salt. *Chin. J. Rock Mech. Eng.* **2010**, *1*, 43–50.
4. Yang, C.; Chen, F.; Zeng, Y. Study on the Creep Damage Relationship of Rock Salt. *Chin. J. Rock Mech. Eng.* **2002**, *21*, 1602–1604.
5. Willson, J.; Poiate, J. Some new findings in salt rocks. *J. Petrol.* **2023**, *39*, 123–134.
6. Yang, C.; Liang, W.; Wei, D.; Yang, H. Feasibility study on underground storage of salt rock energy. *Chin. J. Rock Mech. Eng.* **2005**, *24*, 4409–4417.
7. Charron-Bost, B.; Schiper, A. The heard-of model: Computing in distributed systems with benign faults. *Distrib. Comput.* **2009**, *22*, 49–71. [CrossRef]
8. Pollok, L.; Saßnowski, M.; Kühnlenz, T.; Gundelach, V.; Hammer, J.; Pritzkow, C. Geological exploration and 3D model of the Asse salt structure for SE expansion of the Asse II mine. *Mech. Behav. Salt* **2018**, *9*, 753–763.
9. Yan, C.; Li, Y.; Yan, X.; Cheng, Y.; Han, Z.; Tian, W.; Ren, X. Wellbore shrinkage during drilling in methane hydrate reservoirs. *Energy Sci. Eng.* **2019**, *7*, 930–942. [CrossRef]
10. Reisabadi, M.Z.; Haghighi, M.; Sayyafzadeh, M.; Khaksar, A. Effect of matrix shrinkage on wellbore stresses in coal seam gas: An example from Bowen Basin, east Australia. *J. Nat. Gas Sci. Eng.* **2020**, *77*, 103280. [CrossRef]
11. Fang, X.; Feng, H.; Li, F.; Wang, H. Experimental investigation of the mechanical properties of mud shale under water-bearing conditions and its applications. *Sci. Rep.* **2022**, *12*, 9486. [CrossRef]
12. Fokker, A.F. *Elasticity and Strength of Natural Rock Salts*; Hardy, M.L., Ed.; Trans Tech Publications: Clausthal-Zellerfeld, Germany, 1981; p. 271283.
13. Hunsche, U. True triaxial tests on cubic rock salt samples-experimental methods and results. In *Finite Inelastic Deformations—Theory and Applications: IUTAM Symposium*; Besdo, D., Stein, E., Eds.; Springer: Berlin/Heidelberg, Germany, 1992; pp. 525–536.
14. Hou, M.; Wu, W. Improvement of design of storage cavity in rock salt by using the Hou/Lux constitutive model with consideration of creep rupture criterion and damage. *Chin. J. Geotech. Eng.* **2003**, *25*, 105–108.
15. Tang, M.; Wang, Y.; Ding, G.; Ran, L. Experimental Study and Constitutive Model of the Creep Characteristics of Bedded Rock Salt. *J. China Coal Soc.* **2010**, *1*, 42–45.
16. Aadnoy, B.S. Geomechanical Analysis for Deep-Water Drilling. In *SPE/IADC Drilling Conference and Exhibition*; IADC/SPE 39339; SPE: Dallas, TX, USA, 1998.
17. Rocha, L.A.; Falcão, J.L.; Gonçalves, C.J.C.; Toledo, C.; Lobato, K.; Leal, S.; Lobato, H. Frature Pressure Gradient in Deepwater. In *IADC/SPE Asia Pacific Drilling Technology Conference and Exhibition*; IADC/SPE 88011; SPE: Dallas, TX, USA, 2004.
18. Kaarstad, E.; Aadnoy, B.S. Fracture Model for General Offshore Applications. In *SPE Asia Pacific Oil and Gas Conference and Exhibition*; SPE 101178; SPE: Dallas, TX, USA, 2006.
19. Yang, H.; Chen, M.; Jin, Y.; Xiao, H. Study on the Dynamic Variation of External Casing Pressure in Composite Salt Layers. *Pet. Drill. Tech.* **2006**, *34*, 21–23.
20. Deng, J.; Tian, H.; Wang, Z.; Zhou, J. Experimental Study on the Characteristics of Oil Well Casings Under Uneven External Loads. *Geotech. Mech.* **2005**, *26*, 855–858.
21. Yan, Z.; Wei, K.; Zhai, X.; Liu, Y.; Zhang, L. New Cementing Technology for Fractured Hydrocarbon Reservoirs Based on 2D Spiral Circumferential Vortex. *Nat. Gas Ind.* **2023**, *43*, 71–77.

22. Yin, Y.; Cai, Y.E.; Chen, Z.; Liu, J. Theoretical Solution of Casing Load in Non-uniform Stress Field. *J. Pet.* **2006**, *27*, 133.
23. Zhang, J.; Wang, X. Evaluation of Cement Slurry and Spacer Fluid Properties for Salt-Gypsum Layer Cementing in Y Oilfield. *Chem. Eng.* **2022**, *36*, 58–62+41.
24. Liang, W.G.; Yang, C.H.; Zhao, Y.S.; Dusseault, M.B.; Liu, J. Experimental investigation of mechanical properties of bedded salt rock. *Int. J. Rock Mech. Min. Sci.* **2007**, *44*, 400–411. [CrossRef]
25. Bu, Y.; Liu, H.; Song, W. Experimental Study on the Effect of Lattice Expansion Agents on the Bonding Performance of Cement-Casing Interfaces. *Acta Pet. Sin.* **2011**, *32*, 1067.
26. Chen, X.; Li, B.; Zhang, X.; Wang, Y.; Liu, Q.; Zhao, M.; Xu, F.; Li, J. Application and Insights of Reaming Drilling Technology in the Salt-Gypsum Layers of the Tarim Foreland. *West. Explor. Eng.* **2022**, *34*, 96–99+103.
27. Jin, D. Practical Application of High-Pressure Salt-Gypsum Layer Directional Drilling Technology in the Amu Darya Region of Turkmenistan. *West. Explor. Eng.* **2022**, *34*, 61–62+65.
28. Ma, Y.; Chen, M.; Jin, Y.; Hou, B.; Yang, P. Mechanism Study of the Effect of Relative Humidity on the Creep Behavior of Gypsum Rock. *Pet. Drill. Tech.* **2013**, *41*, 19–22.
29. Zhang, X.; Li, C.; Heng, X.; Zhao, Y.; Wang, H. Challenges and Technical Countermeasures for Cementing in Salt-Gypsum Layers of the Tarim Foreland. *West. Explor. Eng.* **2021**, *33*, 48–52.
30. Zou, S.; Xiong, Y.; Zhang, T.; Wang, Z.; Li, Q.; Liu, H.; Chen, L. Research and Application of Water-Reducing Agent for Cementing in Salt-Gypsum Layers. *Drill. Fluids Complet. Fluids* **2021**, *38*, 765–770.
31. Liu, H.; Wang, W.; Wan, S. Optimization and Field Application of Grading Collar Selection in the Salt-Gypsum Layers of M Oilfield. *Chem. Ind. Manag.* **2021**, *31*, 194–195+198.
32. Wang, J.; Xiong, Y.; Lu, Z.; Zhang, L.; Li, B.; Zhao, X. Salt-Resistant High-Density Cement Slurry Technology for Ultra-Deep Wells. *Drill. Fluids Complet. Fluids* **2021**, *38*, 634–640.
33. Hunsche, U.; Hampel, A. Rock salt—The mechanical properties of the host rock material for a radioactive waste repository. *Eng. Geol.* **1999**, *52*, 271–291. [CrossRef]
34. Gunther, R.M.; Salzer, K.; Popp, T.; Lüdeling, C. Steady-state creep of rock salt: Improved approaches for lab determination and modelling. *Rock Mech. Rock Eng.* **2015**, *48*, 2603–2613. [CrossRef]
35. Tang, W.; Yu, J.; Bin, G. Brief Analysis of Cementing Technology Applications in Deep and Ultra-Deep Wells. *West. Explor. Eng.* **2021**, *33*, 31–33.
36. Liu, W.; Dong, Y.; Zhang, Z.; Li, L.; Jiang, D.; Fan, J.; Chen, J.; Zhang, X.; Wan, J.; Li, Z. Optimization of operating pressure of hydrogen storage salt cavern in bedded salt rock with multi-interlayers. *Int. J. Hydrogen Energy* **2024**, *58*, 974–986. [CrossRef]
37. Tan, M.; Li, Y.; Qi, M.; Wang, H.; Wang, Y.; Lu, J.; Chen, M.; Wu, H. A novel multi-path sand-control screen and its application in gravel packing of deepwater horizontal gas wells. *Nat. Gas Ind. B* **2022**, *9*, 376–382. [CrossRef]
38. Mohammadi, S.; Sedaghatzadeh, M.; Pourafshary, P. Solid-geo-mechanical investigation of the effect of salt creep on casing stability using finite element method: A case study. *SN Appl. Sci.* **2020**, *2*, 1–9. [CrossRef]
39. Taheri, S.R.; Pak, A.; Shad, S.; Mehrgini, B.; Razifar, M. Investigation of rock salt layer creep and its effects on casing collapse. *Int. J. Min. Sci. Technol.* **2020**, *30*, 357–365. [CrossRef]
40. Ghasemi, M.F.; Mehrpooya, M.; Ghiasi, M.M.; Mohammadi, A.H.; Zendehboudi, S. Regional tectonic state and poro-thermo-elasticity analysis of near wellbore zone in field development plan: Utilization of an uncoupled approach. *J. Nat. Gas Sci. Eng.* **2017**, *46*, 615–636. [CrossRef]

Disclaimer/Publisher's Note: The statements, opinions and data contained in all publications are solely those of the individual author(s) and contributor(s) and not of MDPI and/or the editor(s). MDPI and/or the editor(s) disclaim responsibility for any injury to people or property resulting from any ideas, methods, instructions or products referred to in the content.